Journal of the Optical Society of America B
OPTICAL PHYSICS

Anomalous zero-group-velocity photonic bonding states with local chirality

Moïse Sotto,[1] Kapil Debnath,[2,3] Ali Z. Khokhar,[2] Isao Tomita,[1,4] David Thomson,[2] and Shinichi Saito[1,*]

[1]Sustainable Electronic Technologies, Electronics and Computer Science, Faculty of Physical Sciences and Engineering, University of Southampton, University Road, SO17 1BJ Southampton, UK
[2]Optoelectronics Research Centre, Faculty of Physical Sciences & Engineering, University of Southampton, Highfield Campus, Southampton SO17 1BJ, UK
[3]Department of Electronics & Electrical Communication Engineering, Indian Institute of Technology Kharagpur, Kharagpur, West Bengal 721302, India
[4]Department of Electrical & Computer Engineering, National Institute of Technology, Gifu College, Motosu, Japan
*Corresponding author: S.Saito@soton.ac.uk

Received 27 April 2018; revised 19 June 2018; accepted 16 July 2018; posted 18 July 2018 (Doc. ID 330361); published 4 September 2018

Photonic crystal waveguides (PCWs) are promising candidates for the basic building blocks of quantum information processing because they support circular polarization points that can unbalance the directionality of an integrated quantum emitter (QE). Nevertheless, the Purcell effect at circular polarization points saturates near the band edge, the preferred region for quantum electrodynamics. Consequently, chirality and ultra-strong light–matter interaction are difficult to combine. Here, we detract from the vicinity of the band edge, and couple modes with different parities by breaking the mirror symmetry. Using the three-dimensional finite-difference time-domain method, simulated band structures of the implemented photonic bonding states (PBS) display single-mode anomalous zero-group-velocity (ZGV) points far from the band edge. The electric field patterns of these points feature circular polarization points at high field intensity regions where a QE would acquire uni-directional emission behavior. Fabricated devices in silicon (Si) slabs demonstrate the predicted coupling energy between the modes and the signature of single-mode anomalous ZGV points. This method to engineer PBS in PCWs paves the way for outperforming chiral light–matter experiments on-chip.

OCIS codes: (130.5296) Photonic crystal waveguides; (260.5430) Polarization; (270.5580) Quantum electrodynamics.
https://doi.org/10.1364/JOSAB.35.002356

1. INTRODUCTION

There are great expectations that photonic crystal waveguides (PCWs) may serve as the platform of quantum information processing on-chip. Due to their photonic bandgap (BG) [1], PCWs provide a drastic enhancement of the spontaneous emission of an embedded quantum emitter (QE) [2–6]. This is attributed to the tight confinement and the slow-down effect (n_g the group index) of the light. Due to this, the decay rate of the QE into radiative modes outside of the platform is greatly suppressed. The Purcell factor (P_f) is the figure of merit for the effect of the photonic environment on the spontaneous emission [7–9]. In addition to the light–matter interaction enhancement, the BG confinement implies that transverse electric (TE) guided modes in PCWs possess both transverse and longitudinal electric field components. The phase relation between these components involves local chirality across the PCW unit cell, which is characterized by circular polarization points in their field patterns [10,11]. Therefore, an embedded QE with spin-dependent optical transitions at such a particular position infers a non-time-reversal symmetry to the coupled system, and directional factors >90% have been experimentally demonstrated [6]. However, conventional PCWs with mirror symmetry, as shown in Fig. 1(a), prevent the overlap of high field intensity regions and in-plane circular polarization points. Non-symmorphic PCWs like glide-plane waveguides [6,12–14], where one side of the waveguides is shifted along the direction of propagation [Fig. 1(b)], break this paradigm and enhance the electric field intensity of the circular polarization points.

Despite the set of advantages conferred by PCWs, chiral light–matter interaction using this platform is hampered by the self-limitation of utilizing the guided mode near the

band edge. Due to the fact that the chirality is vanishing everywhere in the vicinity of the Brillouin zone (BZ) edge [15], P_f at circular polarization locations inherently saturates near this point [13]. So far, glide-plane waveguides, engineered to unify local chirality and light–matter interaction, are constrained to either moderate n_g values <100 [14] (limiting the coupling) or multi-mode operation [13] (annihilating the uni-directionality). Other methods are needed to force these properties to work in unison and overcome the competition between the vanishing of chirality and the increase of the slow light effect at the band edge. One unexplored approach is to bring the slow-down effect inside the BZ.

In this work, we propose to achieve such a regime by establishing single-mode zero-group-velocity (ZGV) points inside the BZ. The PCW is designed such as bands with different parities are intersecting below the light line and propagate in opposite direction. Thus, the break of the parity ensures branch exchange leading to anomalous ZGV points ($n_g \to \infty$) where the chirality is prevented to vanish.

We start by presenting the wave properties of ZGV points and their consequences on the chiral light–matter interaction enhancement. We emphasize the substitution of the mirror symmetry with glide-plane axes and its impact on the band structure. Particular attention is paid to the emergence of anomalous ZGV points. Then, experimental observation of the photonic bonding states (PBS) is achieved from fabricated silicon (Si) PCWs. The coupling between the PBS as well as the signatures of the anomalous ZGV points are extracted and compared to the simulation results. In the following section, we investigate the local chirality extent at the anomalous ZGV points through the calculation of the Stokes parameters inside the PCW unit cell. There is a strong interest in the circular polarization resulting from the coupling because, at the crossing point, the studied even and odd modes have their dominant electric field components perpendicular to each other. In the conclusion, we summarize about the merit of bringing the slow-down effect inside the BZ.

This work establishes the foundation for outperforming future quantum electrodynamics (QED) experiments on-chip combining a divergent photonic local density of states with extended local chirality.

2. EXTENT OF CIRCULAR POLARIZATION AT ZGV POINTS

For a TE mode in a PCW of lattice constant a as shown in Fig. 1, the electric field components of a circular polarization point obey the relation

$$E_x = \pm iE_y, \tag{1}$$

where $E_x(E_y)$ is the longitudinal (transverse) electric field component, and + (–) stands for right-handed (left-handed) polarization. Nevertheless, the extent of the circular polarization strongly depends on the wave vector of the guided modes. It has a significant importance on the prominence of these points, especially near the boundary of the BZ. Due to the periodicity and the time reversal symmetry of the Maxwell equations, it follows that at the band edge ($k = \pi/a$), the field envelop Ψ can be transformed as

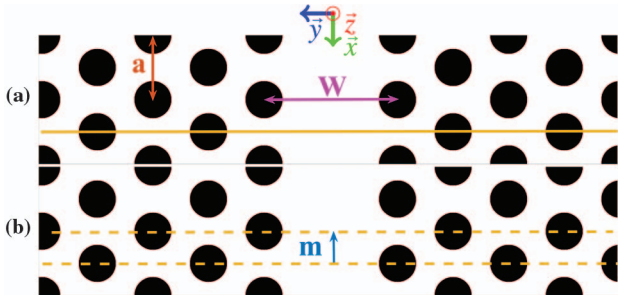

Fig. 1. Schematic of the PCWs with lattice constant a, the waveguide width W (i.e., the distance between the center of the first circular hole rows). The figures introduce the definition of the mismatch m between both parts of the PhC regions. (a) For no mismatch, the structure can be constructed with one side and its mirror image by the plane $(\widehat{xOz})$ placed at $y = 0$. (b) For a mismatch m, one side has been translated by a distance m along the propagation axis. Presented here is the maximum mismatch $m/a = 0.5$.

$$\Psi_{\pi/a}(x,y,z) = \Psi^*_{-\pi/a}(x,y,z) = \Psi^*_{-\pi/a+2\pi/a}(x,y,z) = \Psi^*_{\pi/a}(x,y,z), \tag{2}$$

which states that the field envelop is real at this high symmetry point. On the other hand, the light–matter interaction at the position $\vec{r} = (x,y,z)$, characterized by P_f, is directly proportional to the local density of photonic states [16]:

$$P_f(\vec{r}) \propto |n_g|E^2(\vec{r}), \tag{3}$$

where the electric field is normalized by $\int_{\text{cell}}^{\text{unit}} \epsilon(\vec{r})\vec{E}^2(\vec{r})\mathrm{d}\vec{r} = 1$.

The slow-down effect at the band edge is coming from the interference between backward and forward waves that have the same envelops. This standing wave characteristic states what impedes the use of the band edge for chiral QED experiments: circular polarization locations, denoted $\vec{r}_c$, do not exist for this wave vector. Consequently, the local density of photonic states of these points reaches its maximum before the group velocity diverges and the asymptotic behavior of $|n_g|E^2(\vec{r}_c)$ in the vicinity of the BZ implies that [13,15]

$$\lim_{k \to \frac{\pi}{a}} P_f(\vec{r}_c) \to 0. \tag{4}$$

On the other hand, for a wave vector inside the Brillouin zone ($0 < K < \pi/a$), the Bloch theorem,

$$\Psi_K(x+a,y,z) = \Psi_K(x,y,z)e^{-iKa}, \tag{5}$$

implies that the field envelop must be complex due to the phase shift caused by a translation of one period, regardless of the group velocity. ZGV points at such anomalous positions are of special interest as their properties detract from general standing wave characteristics [15,17–21], because their wave vectors are not associated with a high symmetry point in the BZ. Only such a mode allows the local density of photonic states of circular polarization points $|n_g|E^2(\vec{r}_c)$ to diverge. However, it is important that these anomalous ZGV points are single-mode (i.e., unique in frequency) in order to ensure chiral behavior. Previous works have shown that multi-mode operation annihilated chirality. This is due to the contributions of different wave vectors for which opposite group velocities and/or opposite

circular polarizations are destructively interfering with each other to degrade the local chirality [13]. In the following section, the implementation and the identification of single-mode anomalous ZGV points inside the telecom bandwidth are presented.

3. BAND STRUCTURE OF THE PHOTONIC BONDING STATES

The transformation of the band structure as one side of the photonic crystal (PhC) is shifted by a distance m along the propagation direction [Fig. 1(b)] is represented in Fig. 2. The PhC studied here is a triangular lattice patterned with circular holes of radius $r = 0.29a$ in a 220 nm thick Si membrane. The width of the waveguide (the center-to-center distance of the first rows of holes) is $W = 1.2a\sqrt{3}$ and $a = 450$ nm. The photonic band structures of the TE guided modes were calculated by the three-dimensional finite-difference time-domain method for the *so-called* mismatch parameter "m/a" from 0 to 0.5 in steps of 0.125.

A. Emergence of Anomalous ZGV Points

In the symmorphic waveguide ($m/a = 0$) [Fig. 1(a)], the bands are plotted as solid and dashed black lines for odd and even modes, respectively. Due to their different parities under mirror operation,

$$\hat{R}_y E_y(x, y, z) = \pm E_y(x, -y, z), \tag{6}$$

where $\hat{R}_y$ is the reflection operator and + (-) stands for even (odd) parity, these modes are independent and the lowest energy pair of modes intersects at the wave vector $k_0 = 0.3075(2\pi/a)$. At this crossing point, odd and even modes propagate at the same frequency but with opposite sign group velocities. The break of mirror symmetry ($m/a \neq 0$) causes the modes to couple and form the PBS: the bands transit from crossing (between odd and even modes) to anti-crossing behavior, brought forward by the repulsive coupling strength between $TE^{+}_{1(2)}$ and $TE^{-}_{1(2)}$ modes. The branch exchange leads to the emergence of ZGV points at anomalous positions in the BZ, by imposing the TE^{+}_{1} mode to transit from forward- to backward-propagating wave (and vice versa for the TE^{-}_{1} mode).

Along with the energy splitting, the wave vectors of the ZGV points do not stand at k_0. This is attributed to the distinct dispersions of the even and odd modes at k_0 ($|n_{g,\mathrm{odd}}|(k_0) \neq |n_{g,\mathrm{even}}|(k_0)$). Thus, the anomalous ZGV points of each bonding band also repulse each other along the propagation constant axis. Nevertheless, this artefact does not alter the confinement of the anomalous ZGV points. Indeed, the anomalous ZGV points, which will be labeled as k_0^{+} and k_0^{-} for the TE^{+}_{1} and TE^{-}_{1} modes, respectively, remain below the light line, regardless of m/a. Note that because the odd mode is not monotonic, anomalous ZGV points are not single-mode until m/a crosses certain thresholds. These conditions, related to the total density of states at the anomalous ZGV frequency, will be thoroughly explored in the following section with a finer scan of m/a.

If band repulsion has already been theoretically noticed in glide-plane waveguides [12] and experimentally observed in a contra-directional coupler [22], both occurred above the light line. Our work sets a completely new stage for the practical application of propagating PBS with anomalous ZGV points that are truly confined.

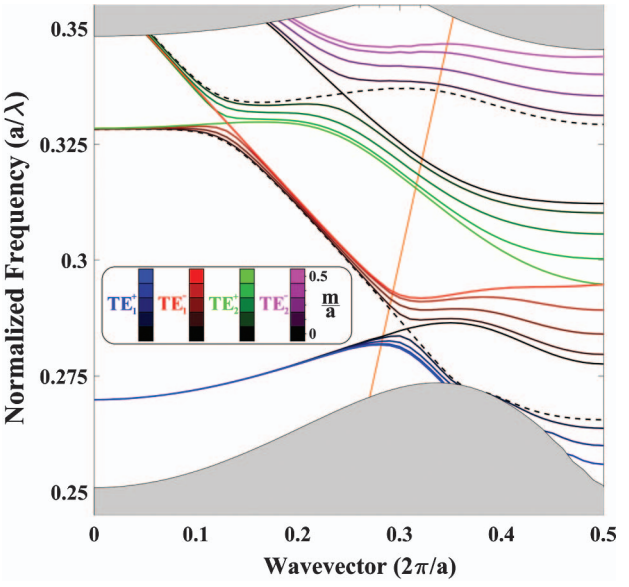

Fig. 2. Photonic band structure of the TE guided modes PCW with the parameters $a = 450$ nm, $W = 1.2\sqrt{3}a$ for different mismatches between PhC sides. The mismatch parameter m/a is scanned from 0 to 0.5 in steps of 0.125. For $m/a = 0$, odd and even modes are respectively represented in solid and dashed black lines. The TE^{+}_{1}, TE^{-}_{1}, TE^{+}_{2}, TE^{-}_{2} modes are represented in shades of blue, red, green, and magenta, respectively. The light line is represented in orange and the PhC bulk modes in gray.

B. On the Origin of the Anti-Crossing

Although the parity is a discrete symmetry, an analogy can be drawn between the coupling phenomenon induced by the mismatch and the coupling of guided modes with same parity [17,23] forced by the periodicity (lack of continuous translational symmetry). In symmorphic PCWs, the order of the guided mode can change from one to another across the same photonic band [1,23]. This is generally accompanied by a sharp transition of the dispersion behavior [23–25]. This effect has been extensively used to tailor the dispersion relation and engineer a dispersionless (constant n_g) bandwidth. By controlling the modal confinement via slight modifications (i.e., the size of the holes of the nearest neighboring rows [26] or their positions [27]), the distribution of the mode orders along the bands is thus altered. Here, the replacement of the mirror symmetry by glide-plane axes implies fortuitous intersections of modes with different parities to split rather than the coupling of modes with same parity induced by the band structure folding (i.e., periodicity).

C. Modes Merging at the BZ Edge

In addition to being repulsed by the TE^{+}_{1} mode, the TE^{-}_{1} mode is also attracted by the TE^{+}_{2} mode until these two modes merge at the band edge for $m/a = 0.5$. As explained in Section 2, the field must be absolutely real at the band edge, regardless of the

PCW symmetry class group. Because the structure is invariant by the glide-plane operation $\hat{G}_m$, it implies that the electric field $\vec{E}_{\vec{k}}$ is an eigenstate of this transformation:

$$\hat{G}_m \vec{E}_{\vec{k}} = \hat{T}_{x=m} \hat{R}_y \vec{E}_{\vec{k}}, \tag{7}$$

where $\hat{T}_{x=m}$ is the translation by m along the propagation axis. Because applying the glide-plane axis symmetry twice is equivalent to a translation of a lattice constant, it follows that for $m/a = 0.5$,

$$\vec{E}_{\pi/a}(x + a/2, -y, z) = \pm i \vec{E}_{\pi/a}(x, y, z), \tag{8}$$

which inhibits the realness of the electric field envelop at the band edge. To ensure the time reversal property at this wave vector, a second mode must merge to counterbalance this extra-phase and satisfies

$$\vec{E}_{1,\pi/a} = \vec{E}^*_{2,\pi/a}. \tag{9}$$

Therefore, all the modes merge in pairs at the band edge to become two-fold degenerate.

4. SPECTROSCOPY OF THE ANOMALOUS ZGV POINTS

In this section, closer insights into the formation of the PBS and the emergence of the anomalous ZGV points are provided through experimental data. If this investigation is strongly motivated by the peculiar dispersion relation of the odd mode, which imposes threshold values on m/a for the anomalous ZGV to be unique in frequency, it also permits measurements of the effective coupling strength. In the previous section, the band structure calculations uncovered that

$$\lambda_{\mathrm{TE}_1^-}\left(\frac{\pi}{a}\right) > \lambda_{\mathrm{TE}_1^+}(k_0^+) \tag{10}$$

for $m/a = 0.125$, meaning that the anomalous ZGV points are multi-mode in this configuration. Nevertheless, as m/a increases, the attraction between the TE_1^- and TE_2^+ modes removes the wavelength degeneracies of the anomalous ZGV points. PCWs with m/a scanned from 0 to 0.5 in steps of 0.05 were fabricated on a silicon-on-insulator wafer. Thereupon, the transmission spectra of the PCWs were measured using a fiber coupler setup. The fabrication process and the measurement setup details are reported in Appendices A and B, respectively. Figure 3 displays the results of the experiment and provides direct access to the repulsive coupling strength as well as unveils the single-mode conditions of the anomalous ZGV points through their relative positions. The simulated wavelengths of the PBS at k_0^+, k_0^- and of the TE_1^- mode at the band edge are superimposed on the measurements as orange, black, and green points, respectively. The wavelength separation between the anomalous ZGV points is a direct measure of the coupling between the PBS. The general behavior and the values are in agreement with simulations, the drops in transmission at k_0^+ and k_0^- are repulsing from each other as m/a is increased, and the simulation windows are blueshifted approximately 0.46% in wavelength to overlap the experimental values. Emphasis may be placed on the induced strong energy splitting measured to be 6.74 THz centered at 191.38 THz for $m/a = 0.5$.

A. Multi-Mode Signature

The anomalous ZGV points take two different signatures in the transmission spectra, depending on if they are single- or multi-mode. In the latter case, ZGV points distinctively appear among the transmission bandwidth due to the multi-mode interference at this precise frequency. They arise in the spectra as clearly local drops of the transmission, due to the non-zero density of state on both sides of these points. This effect is salient due to the ZGV nature of the PBS modes at k_0^+ and k_0^- [20,28]. For instance, at $m/a = 0.15$ the TE_1^- mode at k_0^- is associated with a dip of 25 dDm in the propagation losses. This drastic increase of the optical losses on a such narrow bandwidth is assigned to the increase of the group index as ZGV points are approached [20,24].

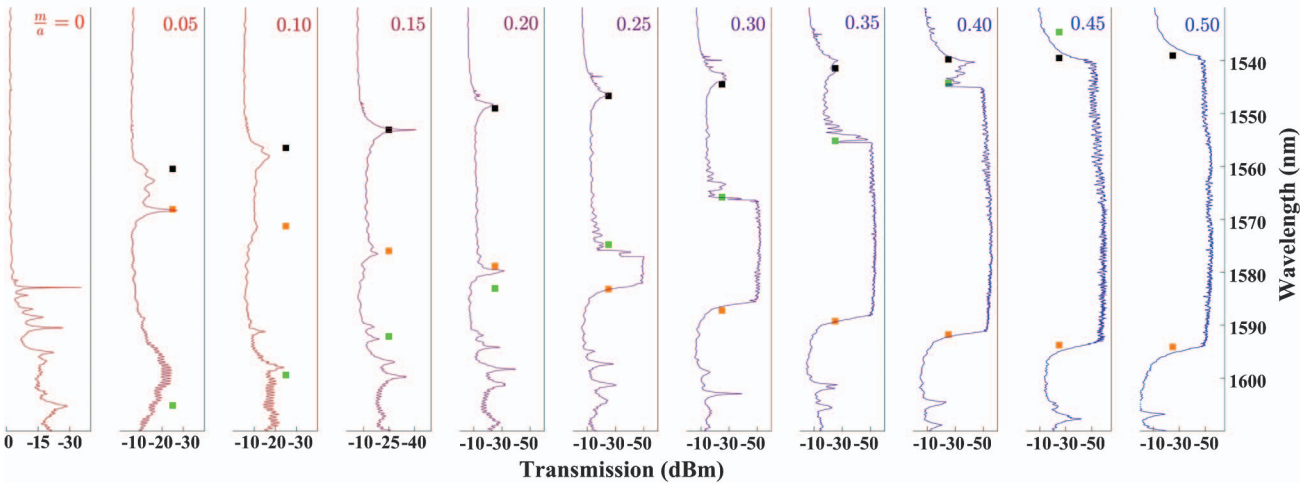

Fig. 3. Normalized transmission spectra of the waveguides with different (m/a) values from 0 (red) to 0.5 (blue) in steps of 0.05. The simulated wavelengths of the anomalous ZGV points (orange and black for bonding and anti-bonding at k_0^+ and k_0^-, respectively) have been superimposed onto the measurements as well as the frequency of the anti-bonding mode at the end of the BZ (in green).

B. Single-Mode Signature

On the other hand, a transition occurs at the m/a values where anomalous ZGV points become single-mode, which is emphasized by the opening of a sub-BG. Therefore, the anomalous ZGV points are associated with the limits of the sub-BG, when they are single-mode. The opening of the sub-BG is subject to both the repulsion of the TE_1^+ and TE_1^- modes at the avoided crossing point and the attraction between TE_1^- and TE_2^+ at the band edge. Thus, two different thresholds are identified.

The TE_1^+ mode at k_0^+ becomes single-mode and the lower limit of the sub-BG for $m/a \geq 0.25$, whereas the TE_1^- mode at k_0^- is single-mode and the upper limit of the sub-BG for $m/a \geq 0.45$.

These transitions from the dips to the limits of the sub-BG predicted by the calculations are matching the experimental values (cf. the relative position of the colored points in Fig. 3).

It can be speculated whether or not the anomalous ZGV points are limited due to their non-zero second-order derivative:

$$\frac{\delta^2}{\delta k^2}\left(\frac{a}{\lambda}\right)_{k_0^{\pm}} \neq 0. \tag{11}$$

These points not only can lead to a significant enhancement of the stimulated emission [29] or be used to design ultra-high quality factor micro-cavity [19], but can also present (under certain conditions) a field intensity rising at the beginning of the propagation [20]. Nevertheless, due to the propagation losses, a coupling into another waveguide is probably preferable for practical applications. To the contrary, if the density of states of zero second-order derivative diverges faster as the anomalous ZGV point is approached [18], their implementation remains challenging. It generally results in the formation of a close pair of anomalous ZGV points with non-zero second-order derivative [20,21], which causes not addressable multi-mode degeneracies. For example, it has a crucial effect on non-linear and laser applications, where the phase matching would be a difficult criterion to engineer.

5. LOCAL CHIRALITY OF THE PBS

Besides introducing dispersion singularities, the mismatch also profoundly alters the electric field profiles. This is especially true at the anomalous ZGV points where the modes with different guidance mechanisms anti-cross. For instance, the odd mode is a gap-guided mode which is well known to have a modal field distribution penetrating several rows of the PhC. The Bragg mechanism enforces this mode to have its dominant electric field component parallel to the propagation. The even mode, for its part, is index guided, its electric field is principally concentrated in the line defect and points in the transverse direction. The fact that the PBS are a combination of such distinct modes constitutes a relevant interest to investigate the resulting polarization. To our knowledge, the effect of branch exchange on the field ellipticity was never explored in previous analysis of non-symmorphic waveguides. Admittedly, the transition between symmorphic and non-symmorphic waveguides results in the discontinuity of many physical properties of the guided modes. For instance, the space group of a non-symmorphic structure does not have the form of a direct product between point and translation groups as the symmorphic PCW [30]. Nevertheless, due to the bonding nature of the PBS, it is relevant to compare them with the odd and even mode profiles at k_0 and investigate the role of m/a on the modification of the field properties.

A. Definition of the Stokes Parameters

In order to point out the local chirality of the anomalous ZGV points, the Stokes parameters [31] S_0 and S_3 of the TE_1^+ and TE_1^- modes at k_0^+ and k_0^-, respectively, have been mapped inside the unit cell of the PCWs with different mismatches. The Stokes parameters S_0 and S_3 are defined as

$$\begin{aligned} S_0(\vec{r}) &= (|E_x(\vec{r})|^2 + |E_y(\vec{r})|^2), \\ S_3(\vec{r}) &= 2\frac{\mathrm{Im}(E_x^*(\vec{r})E_y(\vec{r}))}{S_0(\vec{r})}, \end{aligned} \tag{12}$$

where $\vec{r} = (x, y, z = 0)$. $S_0(\vec{r})$ represents the modal intensity of the electric field [Fig. 4(a)] and $S_3(\vec{r})$ the in-plane polarization ellipticity [Fig. 4(b)]. Circular polarization is depicted by $S_3 = \pm 1$, which represents fully right- and left-handed polarized electric field, respectively. Due to the conservation of the global chirality $S_{3,\vec{k}} = -S_{3,-\vec{k}}$, optical transition of a QE with a specific handedness (i.e., spin dependent) occurring at $|S_3| = 1$ locations will choose a wave vector ($\vec{k}$) rather than its opposite ($-\vec{k}$).

B. Chirality Extent at the Anomalous ZGV Points

In the symmorphic PCW, Fig. 4(b) points out that circular polarization is prevented in the core of the waveguide by the mirror symmetry. Unfortunately, the fields are also mainly concentrated there for the same reason. In contrast, the replacement of the mirror symmetry with the glide-plane symmetries makes this limitation obsolete. It is therefore reasonable to expect the local chirality extent to be significant at k_0^- and k_0^+, exactly where the convolution of the even and odd modes is supposed to be the most prominent. First of all, note that if the PBS exhibit electric field intensity distributions mixing both the even and odd modes, their ellipticity patterns mainly take the aspect of the gap-guided mode outside the line defect. This highlights the strong interaction of the PBS with the PhC bulk due to the mismatch. By increasing m/a, the modal intensities and local chirality patterns morph into undulated shapes, due to the symmetry class of non-symmorphic PCWs [Eq. (7)]. The maximum field intensity region is stretched within the unit cell to respect the glide-plane transformations $\hat{G}_m$ and $\hat{G}_{m-a}$, until it splits into two for $m/a = 0.5$. In order to quantify the overlap of high intensity and circular polarization for both PBS, green crosses indicating $|S_3| = 1$ locations are superimposed on each ellipticity pattern of single-mode anomalous ZGV points.

1. TE_1^+ Mode

If the anomalous ZGV point k_0^+ offers a single-mode operation from $m/a = 0.25$, the $|S_3| = 1$ locations have normalized electric field intensities $S_{0,\mathrm{norm}} = S_0/\max(S_0)$ between 0.27 and 0.33. However, the overlap between modal intensity and local chirality patterns is appreciable. For $m/a = 0.5$, the maximum intensity field point has an ellipticity described

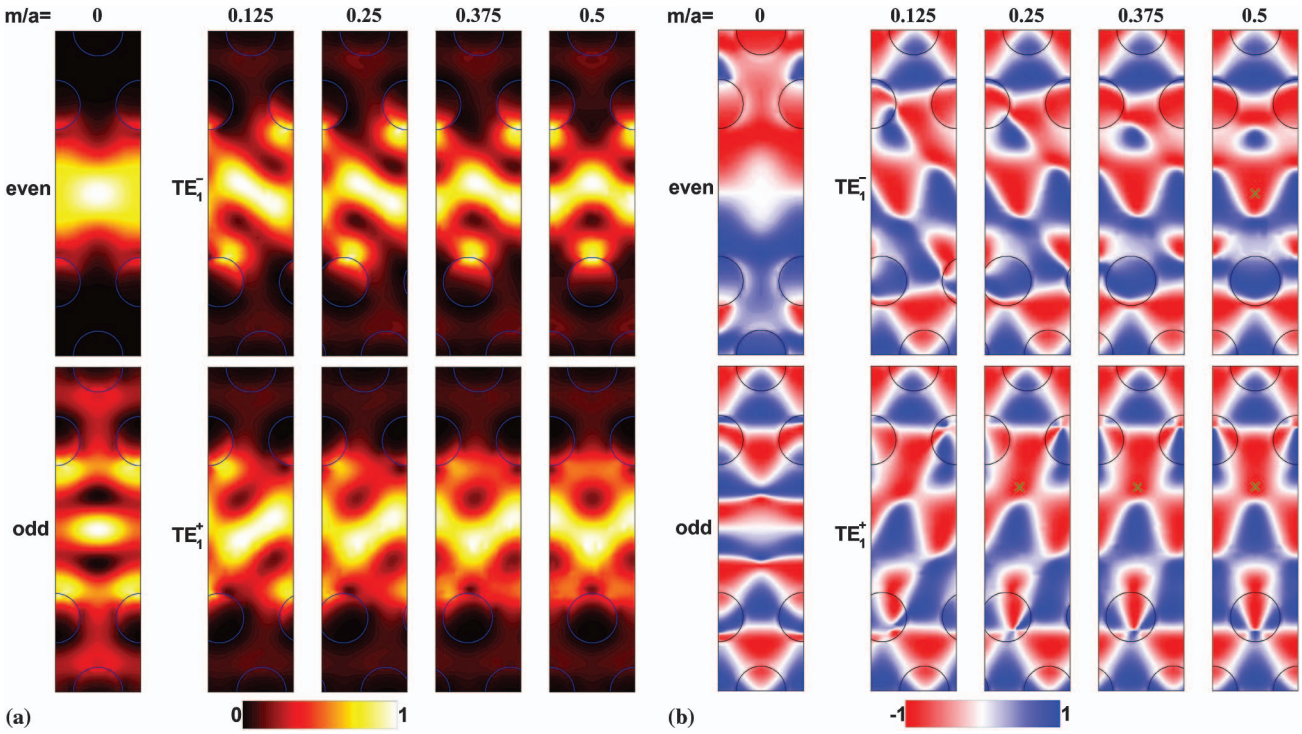

Fig. 4. Relevant properties of the odd and even mode profiles at the k_0 and of TE_1^+ and TE_1^- modes at k_0^+ and k_0^-, respectively. The mismatch parameter m/a has been scanned between 0 and 0.5 in steps of 0.125. (a) The normalized Stokes parameter $S_{0,\mathrm{norm}}(\vec{r}) = (|E_x(\vec{r})|^2 + |E_y(\vec{r})|^2)/\max(|E_x|^2 + |E_y|^2)$. (b) The Stokes parameter $S_3(\vec{r})$, describing the degree of elliptic polarization across the PCWs unit cell. Green crosses have been superimposed at $|S_3| = 1$ positions for mismatches where the anomalous ZGV points are single-mode.

by $|S_3| = 0.78$, while extremely high intensity and nearly unitary directionality are substantiated by points displaying $|S_3| = 0.97$ and $S_{0,\mathrm{norm}} = 0.92$.

2. TE_1^- Mode

On the other hand, the TE_1^- mode at k_0^- displays a strong confinement inside the core of the PCW. It also exhibits enhanced chirality as soon as the mirror symmetry is broken. For $m/a = 0.125$, uni-directional locations have a normalized electric field intensity $S_{0,\mathrm{norm}} = 0.82$. For $m/a = 0.5$, the circular polarization location features $S_{0,\mathrm{norm}} = 0.85$ and the calculated ellipticity of the maximum modal intensity ($S_{0,\mathrm{norm}} = 1$) is $|S_3| = 0.96$. In addition, the field properties were also calculated for $m/a = 0.45$, value for which k_0^- becomes single-mode and for which the $|S_3| = 1$ locations are associated with $S_{0,\mathrm{norm}} = 0.90$. This quantitatively substantiates a strong penetration of the local chirality into high field region for this mode.

The fact remains, however, that the exact use of the anomalous ZGV points could be compromised by the reach of the noise level prior to their wavelengths. Nevertheless, the chiral behavior is not annihilated 1 nm away to the anomalous ZGV point, the maximum multi-mode directionality [13] was calculated to be 0.81.

6. CONCLUSION

To summarize, we presented in this work the design of a non-symmorphic PCW with single-mode anomalous ZGV points supporting circular polarization points. Instead of the general method to work in the vicinity of the band edge, the slow-down effect was forced to exist inside the BZ. This relied on the break of the transversal mirror symmetry inducing a branch exchange between two crossing bands fundamentally opposed, thus resulting in the emergence of ZGV points inside the BZ. Such anomalous position for the slow light prevents the local chirality of the modes from vanishing.

The repulsive coupling strength behavior was probed through transmission measurements on fabricated devices and showed a relative agreement with simulations. The mismatches inducing single-mode anomalous ZGV points were identified by the appearance of a sub-BG contrasting with their multi-modal signature.

By using the Stokes parameters, it has been shown that the coupling of modes, with perpendicular dominant electric field components, is beneficial for implementing circularly polarized location with high electric field intensity. In particular, the TE_1^- mode at k_0^- for $m/a = 0.45$ where circular polarization points are calculated to have a modal intensity $S_{0,\mathrm{norm}} = 0.90$. Hence, QE embedded in the presented platform has the potential to demonstrate strong enhancement of the light–matter interaction with chiral behavior.

On top of that, we believe that the understanding of the formation of these bonding states was summarized to inspire future works in a broad range of domains, not only QED but also all-optical and electro-optic-based devices. Notably, the ultra-strong photonic coupling strength, measured to be

6.74 THz centered at 191.38 THz for $m/a = 0.5$, can also serve to tailor the band structure of guided modes. This magnitude is much stronger than what has been obtained in other purely photonic systems, such as coupled cavities [32], and could be used as the starting point to architect photonic devices where particular tailoring of the dispersion curve is required. The mismatch can be used to balance the even and odd components of the modes along a hybrid band like other dispersion compensation methods [25–27]. It will be beneficial for the community in many aspects to consider glide-plane axis symmetry as a new degree of parametrization and take into account systematic studies of this symmetry during the design of PhC-based devices.

The data from the paper can be obtained from the University of Southampton ePrint research repository: http://DOI:10.5258/SOTON/D0245.

APPENDIX A: FABRICATION

Following our design parameters, in order to observe the signature of the anomalous ZGV points in our different PCWs, we fabricated them on a 220 nm thick ⟨100⟩ silicon-on-insulator wafer by the following major steps. First, the wafer was spin-coated with a 260 nm thick layer of ZEP 520A, a positive e-beam resit. Using e-beam lithography, the patterns were exposed onto the resist, which was then developed with the use of the ZED-N50 developer, and subsequently transferred to the Si layer in an inductively coupled plasma etcher using SF_6/CHF_3 gas chemistry. The remaining resist was removed by an O_2 plasma asher and the surface was cleaned further by fuming nitric acid. Continuously, the sample was dipped in a diluted hydrofluoric acid (HF) to remove native oxide. Then, we spin-coated the sample using a 1.8 μm thick layer of polymethylmethacrylate (PMMA) and windows above the 50 periods long PhC regions were transfered by e-beam lithography. Immediately after the development of the resist in a 1:1 mixed solution of isopropyl alcohol and methyl-isobutyl-ketone, the sample was immersed in HF to remove the buried oxide underneath the Si layer and suspend only the PCWs regions. Thereupon, the PMMA cap was removed by a O_2 plasma asher and the sample was finally dipped in HF to end up with our designed PCWs slabs, as shown Fig. 5.

APPENDIX B: MEASUREMENT SETUP

The transmission spectra were measured by using a fiber coupler setup. The light is originating from a tunable laser source, with a wavelength range from 1530 nm to 1610 nm that completely covers the simulated window of interest. Before reaching the PCWs, the light is coupled to the PhC region using fiber-grating couplers. To ensure the light was TE polarized, it passed through a fiber polarization controller and the gratings were carefully designed to maximize the transmission of this polarization. The wavelength was scanned using the built-in sweeping capability of the laser and the photo-detector automatically recorded each output spectrum. We performed all the measurements by using a 10 dBm laser power. The waveguide transmissions were then normalized by setting the background loss (i.e., setup and coupling loss) to 0 dB using a waveguide without the PhC region.

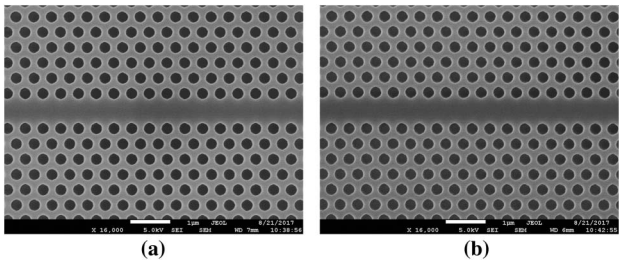

Fig. 5. Scanning electron microscopy imaging of the fabricated devices: (a) no mismatch and (b) $m/a = 1/2$.

Funding. Engineering and Physical Sciences Research Council (EPSRC) (EP/M009416/1, EP/M008975/1); EU FP7 People: Marie-Curie Actions (PEOPLE) (PCIG13-GA-2013-618116); University of Southampton Zepler Institute Research Collaboration Stimulus Fund.

Acknowledgment. The authors would like to acknowledge Daniel Burt, Prof. Harvey Rutt, and Prof. Satoshi Iwamoto for their fruitful discussions.

REFERENCES

1. J. D. Joannopoulos, S. G. Johnson, J. N. Winn, and R. D. Meade, *Photonic Crystals: Molding the Flow of Light* (Princeton University, 2011).
2. H. Nakamura, Y. Sugimoto, K. Kanamoto, N. Ikeda, Y. Tanaka, Y. Nakamura, S. Ohkouchi, Y. Watanabe, K. Inoue, H. Ishikawa, and K. Asakawa, "Ultra-fast photonic crystal/quantum dot all-optical switch for future photonic networks," Opt. Express **12**, 6606–6614 (2004).
3. T. Yoshie, A. Scherer, J. Hendrickson, G. Khitrova, H. Gibbs, G. Rupper, C. Ell, O. Shchekin, and D. Deppe, "Vacuum rabi splitting with a single quantum dot in a photonic crystal nanocavity," Nature **432**, 200–203 (2004).
4. K. Hennessy, A. Badolato, M. Winger, D. Gerace, M. Atature, S. Gulde, S. Falt, E. L. Hu, and A. Imamoglu, "Quantum nature of a strongly coupled single quantum dot cavity system," Nature **445**, 896–899 (2007).
5. M. Arcari, I. Söllner, A. Javadi, S. L. Hansen, S. Mahmoodian, J. Liu, H. Thyrrestrup, E. H. Lee, J. D. Song, S. Stobbe, and P. Lodahl, "Near-unity coupling efficiency of a quantum emitter to a photonic crystal waveguide," Phys. Rev. Lett. **113**, 093603 (2014).
6. I. Söllner, S. Mahmoodian, S. L. Hansen, L. Midolo, A. Javadi, G. Kiršanskė, T. Pregnolato, H. El-Ella, E. H. Lee, J. D. Song, S. Stobbe, and P. Lodahl, "Deterministic photon-emitter coupling in chiral photonic circuits," Nat. Nanotechnol. **10**, 775–778 (2015).
7. E. M. Purcell, *Confined Electrons and Photons* (Springer, 1995).
8. S. Hughes, "Enhanced single-photon emission from quantum dots in photonic crystal waveguides and nanocavities," Opt. Lett. **29**, 2659–2661 (2004).
9. V. M. Rao and S. Hughes, "Single quantum-dot Purcell factor and β factor in a photonic crystal waveguide," Phys. Rev. B **75**, 205437 (2007).
10. M. Burresi, R. Engelen, A. Opheij, D. Van Oosten, D. Mori, T. Baba, and L. Kuipers, "Observation of polarization singularities at the nanoscale," Phys. Rev. Lett. **102**, 033902 (2009).
11. A. B. Young, A. Thijssen, D. M. Beggs, P. Androvitsaneas, L. Kuipers, J. G. Rarity, S. Hughes, and R. Oulton, "Polarization engineering in photonic crystal waveguides for spin-photon entanglers," Phys. Rev. Lett. **115**, 153901 (2015).
12. A. Mock, L. Lu, and J. O'Brien, "Space group theory and Fourier space analysis of two-dimensional photonic crystal waveguides," Phys. Rev. B **81**, 155115 (2010).

13. B. Lang, D. M. Beggs, and R. Oulton, "Time-reversal constraint limits unidirectional photon emission in slow-light photonic crystals," Philos. Trans. R. Soc. A **374**, 20150263 (2016).
14. S. Mahmoodian, K. Prindal-Nielsen, I. Söllner, S. Stobbe, and P. Lodahl, "Engineering chiral light-matter interaction in photonic crystal waveguides with slow light," Opt. Mater. Express **7**, 43–51 (2017).
15. A. A. Sukhorukov, S. Ha, A. S. Desyatnikov, A. V. Lavrinenko, and Y. S. Kivshar, "Slow-light vortices in periodic waveguides," J. Opt. A **11**, 094016 (2009).
16. P. Lodahl, S. Mahmoodian, and S. Stobbe, "Interfacing single photons and single quantum dots with photonic nanostructures," Rev. Mod. Phys. **87**, 347–400 (2015).
17. A. Y. Petrov and M. Eich, "Zero dispersion at small group velocities in photonic crystal waveguides," Appl. Phys. Lett. **85**, 4866–4868 (2004).
18. M. Ibanescu, S. Johnson, D. Roundy, C. Luo, Y. Fink, and J. Joannopoulos, "Anomalous dispersion relations by symmetry breaking in axially uniform waveguides," Phys. Rev. Lett. **92**, 063903 (2004).
19. M. Ibanescu, S. G. Johnson, D. Roundy, Y. Fink, and J. Joannopoulos, "Microcavity confinement based on an anomalous zero group-velocity waveguide mode," Opt. Lett. **30**, 552–554 (2005).
20. M. Spasenović, T. P. White, S. Ha, A. A. Sukhorukov, T. Kampfrath, Y. S. Kivshar, C. M. de Sterke, T. F. Krauss, and L. K. Kuipers, "Experimental observation of evanescent modes at the interface to slow-light photonic crystal waveguides," Opt. Lett. **36**, 1170–1172 (2011).
21. J. Hou, H. Wu, D. Citrin, W. Mo, D. Gao, and Z. Zhou, "Wideband slow light in chirped slot photonic-crystal coupled waveguides," Opt. Express **18**, 10567–10580 (2010).
22. M. Qiu, M. Mulot, M. Swillo, S. Anand, B. Jaskorzynska, A. Karlsson, M. Kamp, and A. Forchel, "Photonic crystal optical filter based on contra-directional waveguide coupling," Appl. Phys. Lett. **83**, 5121–5123 (2003).
23. M. Notomi, A. Shinya, K. Yamada, J.-I. Takahashi, C. Takahashi, and I. Yokohama, "Structural tuning of guiding modes of line-defect waveguides of silicon-on-insulator photonic crystal slabs," IEEE J. Quantum Electron. **38**, 736–742 (2002).
24. M. Notomi, K. Yamada, A. Shinya, J. Takahashi, C. Takahashi, and I. Yokohama, "Extremely large group-velocity dispersion of line-defect waveguides in photonic crystal slabs," Phys. Rev. Lett. **87**, 253902 (2001).
25. L. O'Faolain, S. A. Schulz, D. M. Beggs, T. P. White, M. Spasenović, L. Kuipers, F. Morichetti, A. Melloni, S. Mazoyer, J.-P. Hugonin, and H. Lalanne, "Loss engineered slow light waveguides," Opt. Express **18**, 27627–27638 (2010).
26. L. H. Frandsen, A. V. Lavrinenko, J. Fage-Pedersen, and P. I. Borel, "Photonic crystal waveguides with semi-slow light and tailored dispersion properties," Opt. Express **14**, 9444–9450 (2006).
27. J. Li, T. P. White, L. O'Faolain, A. Gomez-Iglesias, and T. F. Krauss, "Systematic design of flat band slow light in photonic crystal waveguides," Opt. Express **16**, 6227–6232 (2008).
28. W. Liu, D. Yang, G. Shen, H. Tian, and Y. Ji, "Design of ultra compact all-optical XOR, XNOR, NAND and OR gates using photonic crystal multi-mode interference waveguides," Opt. Laser Technol. **50**, 55–64 (2013).
29. K. Sakoda, "Enhanced light amplification due to group-velocity anomaly peculiar to two-and three-dimensional photonic crystals," Opt. Express **4**, 167–176 (1999).
30. C. Bradley and A. Cracknell, *The Mathematical Theory of Symmetry in Solids: Representation Theory for Point Groups and Space Groups* (Oxford University, 2010).
31. G. Milione, H. Sztul, D. Nolan, and R. Alfano, "Higher-order Poincaré sphere, Stokes parameters, and the angular momentum of light," Phys. Rev. Lett. **107**, 053601 (2011).
32. S. Haddadi, P. Hamel, G. Beaudoin, I. Sagnes, C. Sauvan, P. Lalanne, J. A. Levenson, and A. Yacomotti, "Photonic molecules: tailoring the coupling strength and sign," Opt. Express **22**, 12359–12368 (2014).